Article

Highly Effective Covalently Crosslinked Composite Alginate Cryogels for Cationic Dye Removal

Serap Sezen [1], Vijay Kumar Thakur [2,3,4,*] and Mehmet Murat Ozmen [1,*]

1   Department of Bioengineering, Yildiz Technical University, Istanbul 34210, Turkey; seraph@sabanciuniv.edu
2   Biorefining and Advanced Materials Research Centre, SRUC, Edinburgh EH9 3JG, UK
3   Department of Mechanical Engineering, School of Engineering, Shiv Nadar University,
      Greater Noida 201314, Uttar Pradesh, India
4   School of Engineering, University of Petroleum & Energy Studies (UPES),
      Dehradun 248007, Uttarakhand, India
*   Correspondence: Vijay.Thakur@sruc.ac.uk (V.K.T.); ozmenm@yildiz.edu.tr (M.M.O.)

Abstract: Currently, macroporous hydrogels have been receiving attention in wastewater treatment due to their unique structures. As a natural polymer, alginate is used to remove cationic dyes due to its sustainable features such as abundance, low cost, processability, and being environmentally friendly. Herein, alginate/montmorillonite composite macroporous hydrogels (cryogels) with high porosity, mechanical elasticity, and high adsorption yield for methylene blue (MB) were generated by the one-step cryogelation technique. These cryogels were synthesized by adding montmorillonite into gel precursor, followed by chemical cross-linking employing carbodiimide chemistry in a frozen state. The as-prepared adsorbents were analyzed by FT-IR, SEM, gel fraction, swelling, uniaxial compression, and MB adsorption tests. The results indicated that alginate/montmorillonite cryogels exhibited high gelation yield (up to 80%), colossal water uptake capacity, elasticity, and effective dye adsorption capacity (93.7%). Maximum adsorption capacity against MB was 559.94 mg g^{-1} by linear regression of Langmuir model onto experimental data. The Pseudo-Second-Order model was fitted better onto kinetic data compared to the Pseudo-First-Order model. Improved porosity and mechanical elasticity yielding enhanced dye removal capacity make them highly potential alternative adsorbents compared to available alginate/montmorillonite materials for MB removal.

Keywords: alginate; carbodiimide; cryogel; composite; methylene blue; montmorillonite

1. Introduction

In recent years, dye contamination in-ground and freshwaters have been a challenging problem due to their non-biodegradability and toxicity to ecosystems. These effluents are released by industrial applications such as textiles, cosmetics, and plastics [1,2]. Although various synthetic dyes accumulated in nature are toxic, cationic dyes such as methylene blue (MB) (Figure 1) pose more damage to the environment and humans due to their charge [2,3]. Therefore, these unfavorable features of dyes have prompted the development of strategies like photodecomposition, coagulation, flocculation, ion exchange, applying chemical oxidizing agents, and adsorption to remove them from contaminated waters [4–6]. Among all methods, adsorption has been found to be superior in economical and effective ways for the recovery of synthetic dyes owing to the selectivity of adsorbent types, sorbent reusability, and ease of operation [2,4,7,8].

Various materials such as activated carbon, solid agricultural by-products, carbon-based compounds, metallic compounds, polymers, industrial wastes, and clays are applied for dye adsorption in the forms of porous matrices, nanoparticles, membranes, and bulk materials hydrogels [1,5,10]. Hydrogels have been of interest among these materials due to their promising potential in overcoming various ecological, biological, and industrial problems [11,12]. Specifically, hydrogels have been used to remove dyes in polluted water due

to the availability of functional groups for dye attachment, ease of production, processing and handling with a high recovery rate. As a well-known natural polymer-based hydrogel, alginate hydrogel with the advantages of ionic functional groups is commonly utilized to capture ionic dyes [13]. Moreover, alginate hydrogels have been utilized in cationic dye adsorption due to their abundance, being eco-friendly, and low-cost alginate [14]. Alginate is a polysaccharide composed of β-D-Mannuronic Acid (M) and α-L-Guluronic Acid (G) units that possess negatively charged carboxylate groups. Therefore, in divalent cations, alginate forms hydrogel beads by ionic cross-linking [13]. However, these fast ionic cross-linking limits control over the properties of alginate hydrogels, such as porosity and mechanical elasticity due to fast reaction between ionic groups. Generally, the obtained hydrogels possess fast-crosslinked and weak-crosslinked zones that undergo degradation under physiological conditions [15–17]. To eliminate these problems in alginate hydrogels, a covalent cross-linking strategy can be applied.
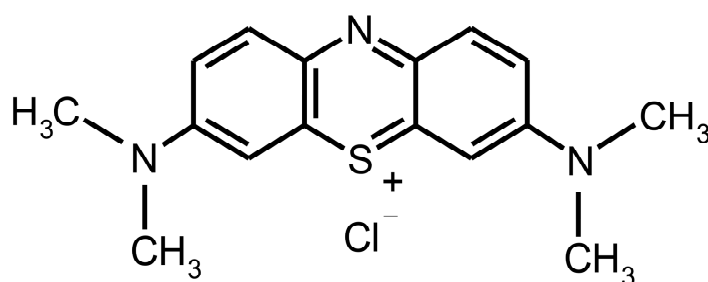

Figure 1. Chemical structure of methylene blue [9].

Recently, cross-linking reaction at low temperature under cooling has been a suggested technique to prepare effective macroporous hydrogels, so-called cryogels. Cryogels are prepared at temperatures below the freezing point of the gelation solvent, where solvent crystals are formed in the semi-frozen system. Subsequently, the reaction system is thawed, leaving micrometer sized large pores [18,19]. Although cryogels have superior swelling and mechanical properties, still a need arises to improve their performance. Incorporating nanomaterials like clay into the cryogel structure can form nanocomposite cryogels with enhanced elasticity, bio-functionality, swelling, antibacterial, and adsorption properties [20–22].

This study prepared alginate/montmorillonite cryogel adsorbent for MB removal by adding montmorillonite clay into polymeric gel precursors of alginate, followed by covalent cross-linking at low temperatures. Crosslinking reaction was achieved with carbodiimide chemistry whereby 1-Ethyl-3-(3-dimethylaminopropyl) carbodiimide (EDC) and N-Hydroxysuccinimide (NHS) were used to activate carboxylate groups of alginate, later cross-linked with cystamine [23,24]. Various alginate materials including alginate cryo-beads for biological applications [25–27], alginate-gelatin cryogels [28], alginate-agarose cryogels and cryo-beads for bioengineering applications [24,29–31], methacrylated alginate cryogels for biomedical applications [32–34], click alginate cryogel for protein delivery [35], covalently cross-linked alginate cryogels for neural tissue engineering by Mooney et al. [36], and alginate quasi-cryogel beads for dye removal by Erim et al. [7,37] were prepared in the form of beads by ionic cross-linking. For instance, alginate/montmorillonite cryogel-like structures were obtained through ionic cross-linking that were designated as quasi-cryogels [7,37]. However, these materials do not exhibit genuine cryogel features as they lack open macroporosity and toughness. Herein, we obtained alginate cryogels in the cylindrical form by chemical cross-linking utilizing EDC/NHS and cystamine crosslinker that could potentially boost the dye removal capacity. A one-step cryogelation technique was applied to generate these novel true alginate/montmorillonite cryogels, and the resulting materials achieved superior dye adsorption capacity compared to available alginate/montmorillonite adsorbents.

2. Results and Discussion

Alginate/MMT composite macroporous gels were prepared using a one-step cryo-gelation method that comprises the preparation of polymeric gel precursor incorporated with MMT clay followed by covalent cross-linking in a moderately frozen state illustrated by Figure 2. Since alginate is a copolymeric polysaccharide owing to carboxylate groups, alginate gels can be formed by amine di-terminated crosslinkers, such as Cys. Therefore, EDC-NHS coupling was also involved in the activation of carboxylate groups, whereby MES was also employed to stabilize the pH of the medium [23,24]. After adding all components into the reaction solution, the mixtures were transferred to cryostat ($-18\,^{\circ}$C) and ice crystal formation during freezing expelled polymer, crosslinker, MMT, and activator. Therefore, cross-linking achieved in the unfrozen phase and later thawing ice crystals revealed macroporous gel structure.
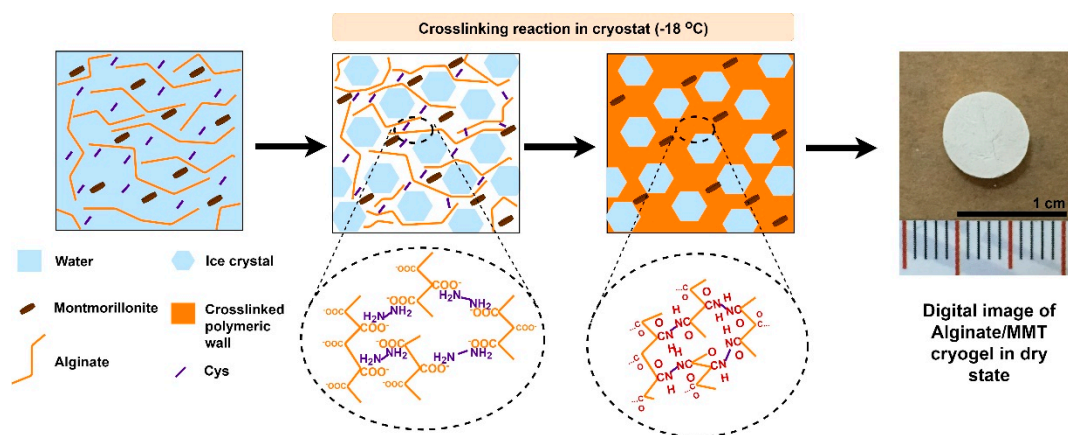

Figure 2. Schematic representation of cryogelation reaction for alginate/MMT macroporous gels and digital image of the dry gel.

2.1. Characterization of Alginate/MMT Cryogels

To investigate the covalent cross-linking reaction between alginate chains and MMT deposition, FT-IR analysis was performed and shown in Figure 3. The spectrum of alginate exhibited broad peaks between 3400 and 3200 cm^{-1}, referring to O-H groups. C-O-O groups were identified as C-O stretching at 1409 cm^{-1} [38]. The peak represented at 1030 cm^{-1} shows O-C-O stretching typical for polysaccharides. The spectra of AMMT0 represents a sharp peak at 1637 cm^{-1}, which corresponds to the amide I bond. Peaks at 1263 and 1568 cm^{-1} show N-H bending of amide II bonds. Amide I and II bonds formation indicates amidation of the carboxylic acid of alginate, meaning that cross-linking of alginate was successfully achieved by Cys [23]. AMMT3 exhibits peaks around 918 cm^{-1} due to Al-Al-O-H stretching of MMT [39]. Therefore, MMT incorporation into alginate cryogels has also been accomplished.

SEM measurements were conducted to investigate the internal morphology of cryogels, as shown in Figure 4a–c. Cryogels showed interconnected macroporous morphology whose pore size can reach 100 μm or more. The incorporation of MMT particles into cryogels imparted roughness to the cryogel surfaces (Figure 4b,c), while smooth topology was observed in AMMT0 (Figure 4a). MMT also reduced pore size due to restriction of ice growth during the freezing process in cryogelation, also reported by Tuncaboylu et al. [40] and Koshy et al. [35]. MMT particles were uniformly distributed through matrices. At the same time, they were mostly entrapped inside pore walls. Pore size and pore size distribution were obtained via Image J analysis on SEM images, shown in Figure 4d. Average pore size for each sample was calculated as 143 ± 55 μm for AMMT0, 121 ± 33 μm for AMMT3 and 114 ± 28 μm for AMMT5 samples, respectively. In conclusion, the average pore size of alginate/MMT samples were gradually decreased with increased MMT amount due to

restriction of ice growth during cryogelation method as a negative replica of the pores [40].
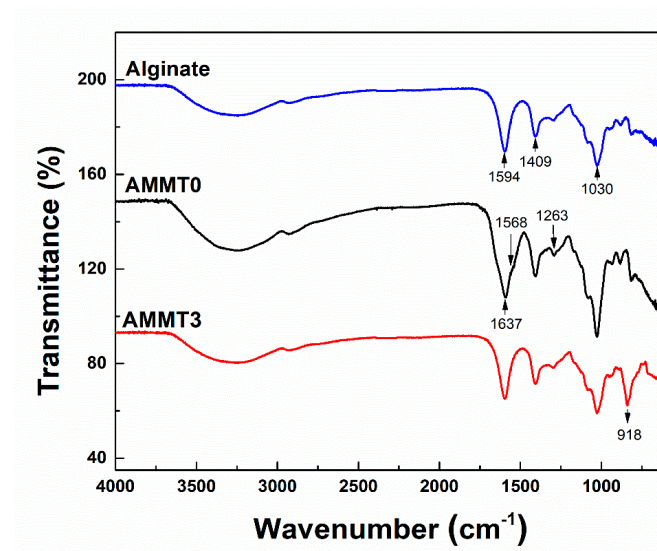

Figure 3. FT-IR spectrum of alginate, AMMT0, and AMMT3 samples. Crosslinking reaction and MMT incorporation were provided by alteration in bands of each specimen.
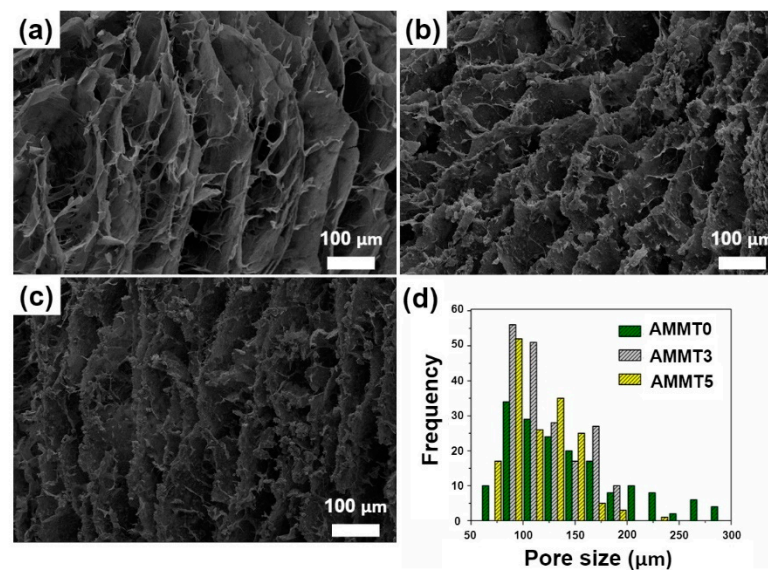

Figure 4. Cross-sectional SEM images and pore size distribution of (**a**) AMMT0, (**b**) AMMT3, and (**c**) AMMT5 samples, (**d**) pore size distribution of each specimen (SEM images were taken in 300× magnification, Scale bar: 100 μm).

Gel fraction (W_g, %) and swelling ratio (q_w) of cryogels as a function of MMT content ((*w/v*) %) were illustrated in Figure 5. The rise in MMT amount slightly decreased the gel fraction of cryogels; however, a sharp decrease in water uptake capacity was recorded. Usually, when gel fraction increases, swelling ratio decreases based on our literature research [1]; however, this observation is mainly reported by gels prepared by ionic cross-linking; therefore, it may be logical to observe these changes in covalently cross-linked networks. The slight decrease in gel fraction could be related to the covering of inorganic particles onto cross-linking points of polymer. The swelling ratio of cryogels decreased by 50% when MMT amount was raised from 0 (*w/v*) % to 5 (*w/v*) %. This is because MMT thickened pore walls and plugged some of the pores available for water flow. The same observations were reported in nanohydroxyapatite-collagen cryogels [41] and aluminum oxide-polyacrylamide cryogels [42].
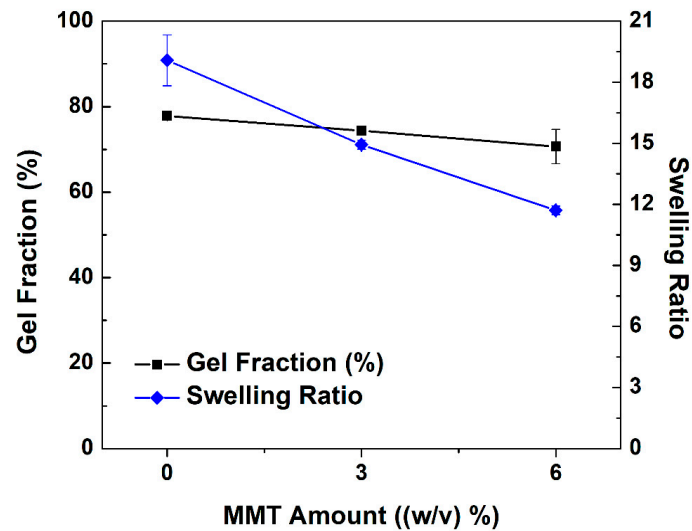
Figure 5. Weight swelling ratio with respect to dry state (q_w) and gel fraction (W_g) (%) of alginate/MMT composite cryogels as a function of MMT content ((*w/v*) %). Measurements completed at least triplicate.

A uniaxial compression test was performed on alginate/MMT composite cryogels to investigate the effect of MMT amount on mechanical behavior. Figure 6 shows the stress–strain curve of each alginate/MMT cryogel. The concave upward curve for elastomeric materials was observed for all cryogels, and they were able to compress up to 80% without any breakage [43]. After the release of load in the compression test, they quickly reabsorbed water released during compression. MMT also enhanced compression stress of the cryogels, whereby their compression limit was attained to 160 kPa stress values. In cryogel systems, denser and thin pore walls yield structural support for these alginate cryogels [44]. Elastic moduli of each cryogel was calculated as 2.387 ± 0.085 kPa for AMMT0, 2.558 ± 0.111 kPa for AMMT3, and 3.697 ± 0.157 kPa for AMMT5, respectively. MMT significantly enhanced elastic moduli, about 1.5 fold, acting as a reinforcing agent. The same observations were reported by Suner et al. [45] and El-Naggar et al. [46], where they reinforced cryogels with clays. Thus, similar stress–strain curves for alginate cryogels were also reported by Kumar et al. [24], whereby they prepared agarose-alginate cryogel for biomedical applications.
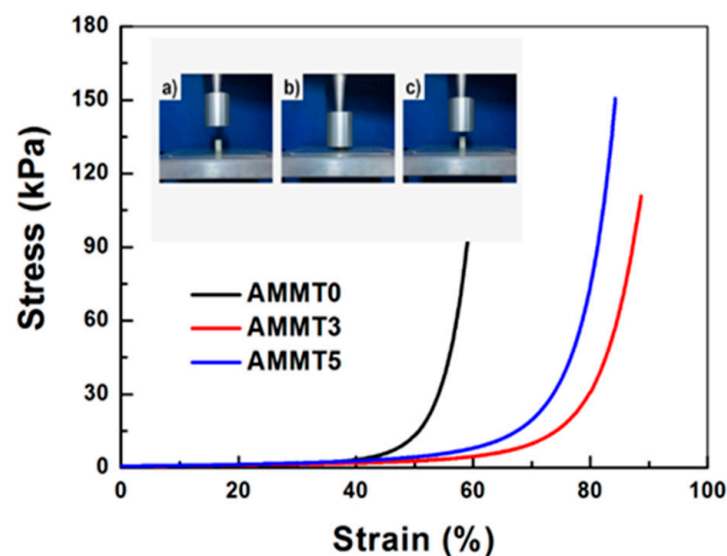

Figure 6. Typical stress–strain curve for AMMT0, AMMT3, and AMMT5 cryogels. (Inset: Digital images of AMMT3 (**a**) before, (**b**) during, and (**c**) after uniaxial compression test).

2.2. Methylene Blue Removal

The impact of MMT content incorporated into cryogels on the MB removal at equilibrium is shown in Figure 7. Since all cryogels exhibited open porous structure and high surface area, they removed up to 90% of the initial MB amount. This can be explained by the cationic nature of MB and the anionic nature of alginate, whereby the gel fraction results also proved that there was still unbound COO⁻ groups for MB attachment [1]. MMT addition also enhanced dye removal by 4% due to negative charges on MMT particles [47]. When the ratio of MMT was overly increased, dye removal was slightly decreased. This could be explained by less water uptake, yielding reduced contact with MB. The decline in removal with the addition of an excess amount of clay is also reported for another adsorbent such as alumina-polyacrylamide composite cryogel [42].
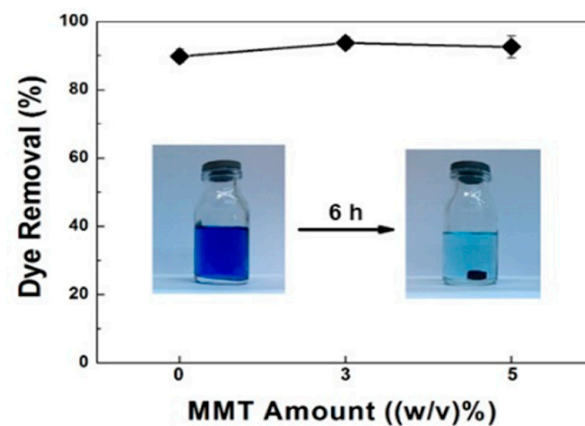

Figure 7. Dye removal (%) by composite cryogels with varying MMT content (inset: digital image of MB solution before (left) and after (right) 6 h contact with sample containing 3 (*w/v*) % of MMT) (initial dye concentration: 25 mg L^{-1}, adsorbent dosage: 0.01 g, experiment duration: 6 h).

A batch adsorption study was conducted to investigate MB's adsorption characteristics by AMMTX composite cryogels. The experimental batch adsorption data and non-linear fitting of isotherm models are illustrated in Figure 8. The highest value of the amount of dye adsorbed per adsorbent in equilibrium was observed with the AMMT3 sample independently of the initial dye concentration. Figure 8 also shows the ''L'' type isotherm, whereby the ratio between dye adsorbed and dye remaining in equilibrium is a concave curve [1]. Langmuir and Freundlich's models were utilized to analyze the relation between dye remaining in solution and dye amount adsorbed onto cryogels in equilibrium. The Langmuir model illustrates uniform and monolayer adsorption through homogeneous surfaces, while the Freundlich model explains heterogeneous adsorption where heat distribution is non-uniform [1]. The non-linear form of Langmuir (Equation (1)) and Freundlich (Equation (2)) models were described as follows:

$$q_e = (q_m K_L C_e)/(1 + K_L C_e) \tag{1}$$

$$q_e = K_F C_e^N \tag{2}$$

where q_m is the maximum adsorption capacity or theoretical adsorption limit of sorbent (mg g^{-1}) and K_L is Langmuir constant (L mg^{-1}) [2]. K_F is Freundlich constant (mg g^{-1}) and N is related to the nature of adsorption. Further, we calculated the feasibility of the adsorption process given by:

$$R_L = 1/(1 + K_L C_i) \tag{3}$$

where R_L is the dimensionless constant, describing the feasibility of the adsorption process [1]. These parameters were calculated by fitting isotherm models onto batch experimental data and illustrated in Table 1.
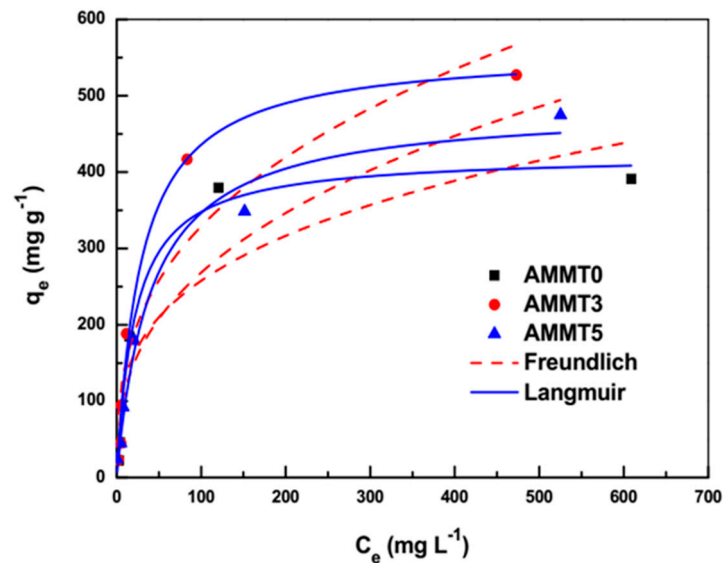
Figure 8. Batch adsorption data of AMMT0, AMMT3, and AMMT5 and non-linear fitting of isotherm models. Batch mode experiments were completed at MB concentrations ranging from 25 to 1000 mg L^{-1}. Adsorbent dosage, MB volume, contact time, and reaction temperature were adjusted to 0.01 g, 0.01 L, 24 h, and 25 °C, respectively.

Table 1. Langmuir and Freundlich isotherm constants for MB adsorption onto composite cryogels.

Cryogel	Langmuir Isotherm	Freundlich Isotherm
AMMT0	q_m (mg g^{-1}), 422.880 K_L (L mg^{-1}), 0.046 R^2, 0.980 R_L, 0.460	K_F, (mg g^{-1}), 65.958 N, 0.296 R^2, 0.790
AMMT3	q_m (mg g^{-1}), 559.950 K_L (L mg^{-1}), 0.035 R^2, 0.981 R_L, 0.530	K_F, (mg g^{-1}), 65.583 N, 0.3502 R^2, 0.870
AMMT5	q_m (mg g^{-1}), 462.770 K_L (L mg^{-1}), 0.028 R^2, 0.990 R_L, 0.590	K_F, (mg g^{-1}), 51.142 N, 0.356 R^2, 0.950

Based on a high correlation coefficient (R^2) that indicates the degree of fitting of isotherm models, the higher value obtained in the Langmuir model, indicating homogenous adsorption, where active sites for dye attachment were equally distributed all over the macroporous networks. The theoretical maximum adsorption capacity for AMMT3 was found as 559.9457 mg g^{-1}, which is relatively high compared to available adsorbents such as poly(vinyl alcohol)-chitosan-alginate-MMT hydrogel beads (137.2 mg g^{-1}) [8], alginate-MMT quasi-cryogel beads (181.8 mg g^{-1}) [7], and alginate-clinoptilolite beads (452.25 mg g^{-1}) [1], cellulose-derived carbon montmorillonite (138 mg g^{-1}) [48], magnetic alginate-rice husk composite (274.9 mg g^{-1}) [13]; however, relatively low compared to adsorbents such as mesoporous synthetic hectorite clay-alginate composite (785.45 mg g^{-1}) [49], calcium alginate-bentonite-activated carbon beads (756.97 mg g^{-1}) [4], alginate-bentonite beads (2024 mg g^{-1}) [50], porous calcium alginate membranes (3506.4 mg g^{-1}) [51]. R_L values are found to be between 1 and 0, indicating that adsorption is favorable for all cryogels.

A kinetic study was completed to understand the mechanism of the adsorption process. Two kinetic models, Pseudo-First Order (PFO) and Pseudo-Second Order (PSO) models, were applied to the data, as shown in Figure 9. As can be seen, all cryogel

reached their equilibrium after about 6 h of contact with the MB solution, whose adsorption capacities reached around 20 mg g^{-1}. The fast removal of MB is obtained due to the open macroporosity of these cryogels, allowing the rapid flow of water and fast diffusion of dye particles [52]. However, extensive amounts of MMT hindered active sites for MB attachment resulting in reduced adsorption capacity.
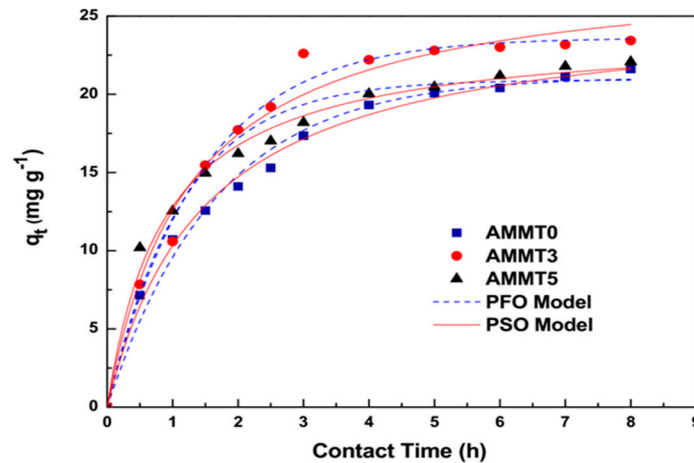

Figure 9. Non-linear regression of kinetic models on the MB retention by AMMT0, AMMT3, and AMMT5 samples (initial dye amount: 25 mg L^{-1}, adsorbent dosage: 0.01 g, temperature: 25 °C, volume: 10 mL).

PFO and PSO kinetic models were employed to characterize adsorption mechanisms of MB by alginate/MMT cryogels. PFO kinetic model favors the physisorption mechanism. The PSO kinetic model is based on the theory that the limiting step of adsorption rate covers the sharing or transfer of electrons between adsorbent and sorbent. Non-linear forms of PFO and PSO kinetic models are illustrated by Equations (4) and (5), respectively:

$$q_t = q_e(1 + e^{-k_1 t}) \tag{4}$$

$$q_t = (k_2 q_e^2 t)/(1 + q_e k_2 t) \tag{5}$$

where q_e is the adsorption capacity of cryogels in equilibrium (mg g^{-1}), k_1 is PFO rate constant (h^{-1}), and k_2 is PSO rate constant, respectively [1]. The parameters of kinetic models calculated from experimental data are shown in Table 2. Considering high R^2 values, adsorption of MB is better described by PSO kinetic model, revealing that adsorption of MB onto cryogels has a rate-limiting step [1]. In accordance, it was also determined in previous studies where alginate-MMT quasi-cryogel beads and alginate/bentonite composite were applied for MB removal that PSO kinetic model well describes the MB adsorption [7,53].

Table 2. PFO and PSO kinetic parameters for MB adsorption onto AMMT0, AMMT3, and AMMT5 samples at the initial dye concentration of 25 mg L^{-1}.

Cryogel	PFO Kinetic Model	PSO Kinetic Model
AMMT0	$q_{e,calc}$ (mg g^{-1}), 21.13 k_1 (min^{-1}), 0.010 R^2, 0.980	$q_{e,calc}$ (mg g^{-1}), 25.62 k_2 (min^{-1}), 0.004 R^2, 0.990
AMMT3	$q_{e,calc}$ (mg g^{-1}), 23.62 k_1 (min^{-1}), 0.017 R^2, 0.980	$q_{e,calc}$ (mg g^{-1}), 28.26 k_2 (min^{-1}), 0.005 R^2, 0.980
AMMT5	$q_{e,calc}$ (mg g^{-1}), 20.93 k_1 (min^{-1}), 0.014 R^2, 0.960	$q_{e,calc}$ (mg g^{-1}), 24.07 k_2 (min^{-1}), 0.008 R^2, 0.990

3. Conclusions

Macroporous hydrogels, so-called cryogels, are sustainable materials for wastewater treatment. In the current study, we prepared alginate cryogels with a one-step cryogelation technique. Additionally, MMT was incorporated into alginate cryogels to improve mechanical strength and dye removal performance. For the cryogelation reaction, we benefitted from carbodiimide chemistry to cross-link carboxylic groups on the alginate with di-amine terminated cystamine. Unlike the calcium cross-linked cryogel-like structures of the alginate, these cryogels exhibited interconnected and open porous structures. With the one-step cryogelation technique, any shape of alginate cryogels with homogeneous cross-linking can be prepared via chemical cross-linking in the moderately frozen state. All cryogels exhibited high water uptake capacity and gel fraction values. While MMT decreased water retention capacity, it enhanced the mechanical elasticity and elastic modulus of the alginate cryogels. MMT also improved dye removal capacity against MB, which was found as 93.7%. The Langmuir model was more suitable to explain MB adsorption, whereby homogenous adsorption was observed. The maximum adsorption capacity was found as 559.74 g g^{-1}, which is a relatively high value compared to other alginate/MMT adsorbents. Adsorption of MB onto alginate/MTT cryogels were better described by the Pseudo-Second Order kinetic model, revealed by the linear regression of kinetic models onto experimental data. Therefore, we can conclude that these macroporous adsorbents can potentially remove cationic dyes from wastewaters.

4. Materials and Methods

4.1. Materials

Alginic acid sodium salt from brown algae (alginate, low viscosity, Sigma, Tokyo, Japan), N-Hydroxysuccinimide (NHS, Sigma, Tokyo, Japan), 2-(N-Morpholino) ethane sulfonic acid hydrate (MES, Sigma, Tokyo, Japan), Cystamine hydrochloride (Cys, Sigma, Tokyo, Japan), N-(3-Dimethylaminopropyl)-N′-ethyl carbodiimide hydrochloride (EDC, Sigma, Tokyo, Japan), Montmorillonite K10 (MMT, Sigma, Tokyo, Japan), and Methylene blue (MB, Sigma, Tokyo, Japan) were used as received. The Milli-Q system supplied distilled water in all experiments. The molecular weight of alginate was found as 110 kDa by gel permeation chromatography analysis.

4.2. Preparation of Alginate/MMT Cryogels

Specific amounts of alginate, 28 mg NHS and 62 mg MES were dissolved in 2 mL of distilled water to obtain the molar ratio of COO-:NHS as 2:1, and a suitable amount of MMT was also added into this mixture and mixed for 40 min at 25 °C. Later, a fresh solution of 112 mg Cys in 100 μL distilled water was added into the solution and further mixed for 10 more minutes. A certain amount of EDC was added, mixed quickly, and transferred into disposable syringes, then replaced into cryostat at −18 °C for cryogelation of 48 h. The preparation route for alginate/MMT cryogels are shown in Figure 10. In polymeric gel precursor solution, the mole ratio of COO-:NHS:EDC was obtained as 2:1:2. After complete cross-linking, all specimens were removed from molds, washed several times with distilled water, and freeze-dried for further use. Alginate/MMT cryogels were designated as AMMTX, where X refers to the amount of MMT ((*w/v*) %) incorporated into cryogels.

4.3. Characterization of Alginate/MMT Cryogels

We characterized AMMTX cryogels in terms of FT-IR, SEM, gel fraction and swelling, mechanical testing, and adsorbent for MB removal.

FT-IR analysis was performed to ensure cross-linking reactions between alginate chains. IR spectra were recorded by FT-IR spectrophotometer (Shimadzu IR-Prestige 21) with Attenuated Total Reflection (ATR) unit. The spectra of dry samples were taken three times in the wavenumber ranging from 4000 to 650 cm^{-1}. The spectrum was recorded three times for each specimen, whereby each spectrum was recorded after averaging 32 IR scans.
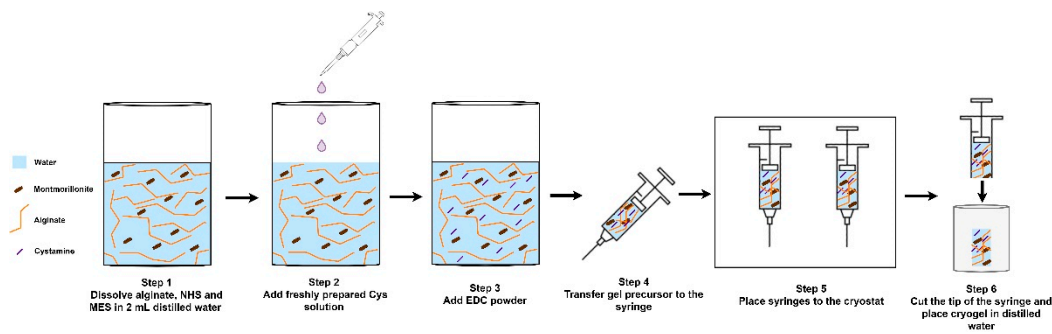
Figure 10. Schematic representation of the preparation of gel precursor of alginate/MMT cryogels and transfer of gel precursor solution to the cryostat.

Scanning Electron Microscopy (SEM, Zeiss EVO LS 10) was used to evaluate the internal morphology of dry cryogels. Before imaging, the specimens were cut with a razor blade then sputter-coated with gold-palladium with a standard protocol (creating 5–10 nm gold-palladium layer). SEM images were taken in secondary electron mode at 20 kV.

To evaluate cross-linking efficiency of cryogels, gel fraction (W_g, %) was calculated by:

$$W_g(\%) = [(M_{dry}/M_0) \times 1/(0.05 \times X_{MMT})] \times 100 \tag{6}$$

where M_0 is the weight of samples after preparation (g), M_{dry} is the weight of dry specimens (g), and X_{MMT} is the fraction (*w/v*) of MMT in the reaction medium [19].

To determine water retention capacity, equilibrium volume and weight swelling ratios of the samples with respect to dry states were calculated. The equilibrium weight-swelling ratio concerning dry states (q_w) of the samples was calculated as:

$$q_w = (M_{sw}/M_{dry}) \tag{7}$$

where M_{sw} is the weight of swollen equilibrium cryogels (g) [19]. All measurements were repeated at least three times at room temperature.

A uniaxial compression test was performed with a load cell via Texture Analyzer TA.HD.Plus (Stable Micro Systems, Godalming, UK) with the computer analyzer system Texture Exponent 32 at room temperature. The compression speed was adjusted at 0.1 mm s^{-1}, and tests were performed up to 80% compression of the original size of the samples in the swollen equilibrium state. The elastic modulus of each specimen was calculated by the slope of the initial linear part of the stress–strain curve [19].

4.4. Dye Removal

Adsorption of MB dye on the specimens was conducted by batch procedure and kinetic study with a magnetic stirring at a speed of 200 rpm at 25 °C. In each experiment, 0.01 gr dry adsorbent was soaked into 10 mL of MB solution. MB concentration in remaining solutes was measured using UV-Vis Spectrophotometer (UV-1700 PharmaSpec, Schimadzu, Kyoto, Japan) at 665 nm [1]. Each experiment was conducted three times.

For the batch procedure, MB solutions were prepared with varying concentrations (25 to 1000 mg L^{-1}), and the experiment was conducted for 24 h. The amount of dye adsorbed in equilibrium (q_e, mg g^{-1}) was calculated by Equation (8):

$$q_e = (C_i - C_e) \times V/M \tag{8}$$

C_i and C_e refer to the dye concentration in aqueous solution before (mg L^{-1}) and after (mg L^{-1}) adsorption. V is the volume of the aqueous medium (L) and M is the dosage of dry adsorbent (g) [2].

A 25 mg L^{-1} MB solution was employed for kinetic study, and an experiment was conducted for 8 h. The amount of dye adsorbed onto cryogels per time (qt, mg g^{-1}) was calculated by Equation (9) given as:

$$qt = (C_i - C_t) \times V/M \tag{9}$$

where C_t refers to the concentration of the MB dye remaining in solution at time t (mg L^{-1}) [2].

Dye removal per sorbent (%) was also calculated using equations as follows:

$$\text{Dye removal (\%)} = (C_i - C_e)/C_i \times 100 \tag{10}$$

where C_i and C_e are the same as Equation (8) [1].

Author Contributions: S.S. completed all experiments, graphs, and drawings; M.M.O. guided the experiments, participated in writing, and interpreted the data obtained from the experiments; V.K.T. extensively revised the manuscript, provided critical revisions, and contributed to the final manuscript. All authors have read and agreed to the published version of the manuscript.

Conflicts of Interest: The authors declare no conflict of interest.

References

1. Ates, B.; Koytepe, S.; Ulu, A.; Gurses, C.; Thakur, V.K. Chemistry, Structures, and Advanced Applications of Nanocomposites from Biorenewable Resources. *Chem. Rev.* **2020**, *120*, 9304–9362. [CrossRef] [PubMed]
2. Raizada, P.; Thakur, P.; Sudhaik, A.; Singh, P.; Thakur, V.K.; Hosseini-Bandegharaei, A. Fabrication of Dual Z-Scheme Photocatalyst via Coupling of BiOBr/Ag/AgCl Heterojunction with P and S Co-Doped g-C3N4 for Efficient Phenol Degradation. *Arab. J. Chem.* **2020**, *13*, 4538–4552. [CrossRef]
3. Singh, P.; Sharma, K.; Hasija, V.; Sharma, V.; Sharma, S.; Raizada, P.; Singh, M.; Saini, A.K.; Hosseini-Bandegharaei, A.; Thakur, V.K. Systematic Review on Applicability of Magnetic Iron Oxides–Integrated Photocatalysts for Degradation of Organic Pollutants in Water. *Mater. Today Chem.* **2019**, *14*, 100186. [CrossRef]
4. Rana, A.K.; Mishra, Y.K.; Gupta, V.K.; Thakur, V.K. Sustainable Materials in the Removal of Pesticides from Contaminated Water: Perspective on Macro to Nanoscale Cellulose. *Sci. Total Environ.* **2021**, *797*, 149129. [CrossRef]
5. Chandel, N.; Sharma, K.; Sudhaik, A.; Raizada, P.; Hosseini-Bandegharaei, A.; Thakur, V.K.; Singh, P. Magnetically Separable ZnO/ZnFe2O4 and ZnO/CoFe2O4 Photocatalysts Supported onto Nitrogen Doped Graphene for Photocatalytic Degradation of Toxic Dyes. *Arab. J. Chem.* **2020**, *13*, 4324–4340. [CrossRef]
6. Rana, A.K.; Frollini, E.; Thakur, V.K. Cellulose Nanocrystals: Pretreatments, Preparation Strategies, and Surface Functionalization. *Int. J. Biol. Macromol.* **2021**, *182*, 1554–1581. [CrossRef]
7. Thakur, V.K.; Voicu, S.I. Recent Advances in Cellulose and Chitosan Based Membranes for Water Purification: A Concise Review. *Carbohydr. Polym.* **2016**, *146*, 148–165. [CrossRef]
8. Thakur, V.K.; Thakur, M.K. Recent Advances in Green Hydrogels from Lignin: A Review. *Int. J. Biol. Macromol.* **2015**, *72*, 834–847. [CrossRef]
9. Pajaie, S.H.S.; Archin, S.; Asadpour, G. Optimization of Process Parameters by Response Surface Methodology for Methylene Blue Removal Using Cellulose Dusts. *Civ. Eng. J.* **2018**, *4*, 620. [CrossRef]
10. Rana, A.K.; Gupta, V.K.; Saini, A.K.; Voicu, S.I.; Abdellattifaand, M.H.; Thakur, V.K. Water Desalination Using Nanocelluloses/Cellulose Derivatives Based Membranes for Sustainable Future. *Desalination* **2021**, *520*, 115359. [CrossRef]
11. Sharma, B.; Thakur, S.; Mamba, G.; Prateek; Gupta, R.K.; Gupta, V.K.; Thakur, V.K. Titania Modified Gum Tragacanth Based Hydrogel Nanocomposite for Water Remediation. *J. Environ. Chem. Eng.* **2020**, 104608. [CrossRef]
12. Thakur, S.; Sharma, B.; Verma, A.; Chaudhary, J.; Tamulevicius, S.; Thakur, V.K. Recent Progress in Sodium Alginate Based Sustainable Hydrogels for Environmental Applications. *J. Clean. Prod.* **2018**, *198*, 143–159. [CrossRef]
13. Verma, A.; Thakur, S.; Mamba, G.; Prateek; Gupta, R.K.; Thakur, P.; Thakur, V.K. Graphite Modified Sodium Alginate Hydrogel Composite for Efficient Removal of Malachite Green Dye. *Int. J. Biol. Macromol.* **2020**, *148*, 1130–1139. [CrossRef]
14. Oussalah, A.; Boukerroui, A.; Amina, A.; Djellouli, B. Cationic and anionic dyes removal by low-cost hybrid alginate/natural bentonite composite beads: Adsorption and reusability studies. *Int. J. Biol. Macromol.* **2019**, *124*, 854–862. [CrossRef] [PubMed]
15. Thakur, S.; Verma, A.; Kumar, V.; Jin Yang, X.; Krishnamurthy, S.; Coulon, F.; Thakur, V.K. Cellulosic Biomass-Based Sustainable Hydrogels for Wastewater Remediation: Chemistry and Prospective. *Fuel* **2022**, *309*, 122114. [CrossRef]
16. Kuo, C.K.; Ma, P.X. Maintaining dimensions and mechanical properties of ionically cross-linked alginate hydrogel scaffolds in vitro. *J. Biomed. Mater. Res. Part A* **2008**, *84A*, 899–907. [CrossRef] [PubMed]

17. Dodero, A.; Pianella, L.; Vicini, S.; Alloisio, M.; Ottonelli, M.; Castellano, M. Alginate-based hydrogels prepared via ionic gelation: An experimental design approach to predict the cross-linking degree. *Eur. Polym. J.* **2019**, *118*, 586–594. [CrossRef]

18. Ozmen, M.M.; Fu, Q.; Kim, J.; Qiao, G.G. A rapid and facile preparation of novel macroporous silicone-based cryogels via photo-induced thiol–ene click chemistry. *Chem. Commun.* **2015**, *51*, 17479–17482. [CrossRef]

19. Sen, T.; Ozcelik, B.; Ozmen, M.M. Tough and hierarchical porous cryogel scaffolds preparation using n-butanol as a non-solvent. *Int. J. Polym. Mater. Polym. Biomater.* **2019**, *68*, 411–416. [CrossRef]

20. Tanc, B.; Orakdogen, N. Charged groups synergically enhanced elasticity and tunable swelling/shrinking of poly(dialkylaminoethyl methacrylate)/layered silicate nanocomposite cryogels. *Polym. (Guildf)* **2019**, *178*, 121627. [CrossRef]

21. Shu, Y.; Huang, R.; Wei, X.; Liu, L.; Jia, Z. Pb(II) Removal Using TiO2-Embedded Monolith Composite Cryogel as an Alternative Wastewater Treatment Method. *Water Air Soil Pollut.* **2017**, *228*, 375. [CrossRef]

22. Loo, S.-L.; Fane, A.G.; Lim, T.-T.; Krantz, W.B.; Liang, Y.-N.; Liu, X.; Hu, X. Superabsorbent Cryogels Decorated with Silver Nanoparticles as a Novel Water Technology for Point-of-Use Disinfection, Environ. *Sci. Technol.* **2013**, *47*, 9363–9371. [CrossRef] [PubMed]

23. Zhao, Y.; Gao, S.; Zhao, S.; Li, Y.; Cheng, L.; Li, J.; Yin, Y. Synthesis and characterization of disulfide-crosslinked alginate hydrogel scaffolds. *Mater. Sci. Eng. C* **2012**, *32*, 2153–2162. [CrossRef]

24. Tripathi, A.; Kumar, A. Multi-Featured Macroporous Agarose–Alginate Cryogel: Synthesis and Characterization for Bioengineering Applications. *Macromol. Biosci.* **2011**, *11*, 22–35. [CrossRef]

25. Shan, L.; Gao, Y.; Zhang, Y.; Yu, W.; Yang, Y.; Shen, S.; Zhang, S.; Zhu, L.; Xu, L.; Tian, B.; et al. Fabrication and Use of Alginate-Based Cryogel Delivery Beads Loaded with Urea and Phosphates as Potential Carriers for Bioremediation. *Ind. Eng. Chem. Res.* **2016**, *55*, 7655–7660. [CrossRef]

26. Fatoni, A.; Dwiasi, D.W.; Hermawan, D. Alginate cryogel based glucose biosensor. *IOP Conf. Ser. Mater. Sci. Eng.* **2016**, *107*, 12010. [CrossRef]

27. Zhang, W.; Yang, Y.; Guan, T.; Guan, J.; Zheng, S.; Chen, B.; Yun, J. Formation Dynamics of Cell-Loading Alginate Droplets in the Microtube Dripping and Cryo-Cross-Linking Process for Cell-Entrapped Cryogel Beads as the Biocatalysts toward Phenyllactic Acid Biosynthesis. *Ind. Eng. Chem. Res.* **2018**, *57*, 7291–7300. [CrossRef]

28. Tripathi, A.; Vishnoi, T.; Singh, D.; Kumar, A. Modulated Crosslinking of Macroporous Polymeric Cryogel Affects In Vitro Cell Adhesion and Growth. *Macromol. Biosci.* **2013**, *13*, 838–850. [CrossRef]

29. Tripathi, A.; Sami, H.; Jain, S.; Viloria-Cols, M.; Zhuravleva, N.; Nilsson, G.; Jungvid, H.; Kumar, A. Improved bio-catalytic conversion by novel immobilization process using cryogel beads to increase solvent production. *Enzyme Microb. Technol.* **2010**, *47*, 44–51. [CrossRef]

30. Tripathi, A.; Melo, J.S.; D'Souza, S.F. Uranium (VI) recovery from aqueous medium using novel floating macroporous alginate-agarose-magnetite cryobeads. *J. Hazard. Mater.* **2013**, *246–247*, 87–95. [CrossRef]

31. Tripathi, A.; Hadapad, A.B.; Hire, R.S.; Melo, J.S.; D'Souza, S.F. Polymeric macroporous formulations for the control release of mosquitocidal Bacillus sphaericus ISPC-8. *Enzyme Microb. Technol.* **2013**, *53*, 398–405. [CrossRef] [PubMed]

32. Bencherif, S.A.; Warren Sands, R.; Ali, O.A.; Li, W.A.; Lewin, S.A.; Braschler, T.M.; Shih, T.-Y.; Verbeke, C.S.; Bhatta, D.; Dranoff, G.; et al. Injectable cryogel-based whole-cell cancer vaccines. *Nat. Commun.* **2015**, *6*, 7556. [CrossRef]

33. Bencherif, S.A.; Sands, R.W.; Bhatta, D.; Arany, P.; Verbeke, C.S.; Edwards, D.A.; Mooney, D.J. Injectable preformed scaffolds with shape-memory properties. *Proc. Natl. Acad. Sci. USA* **2012**, *109*, 19590–19595. [CrossRef] [PubMed]

34. Shih, T.-Y.; Blacklow, S.O.; Li, A.W.; Freedman, B.R.; Bencherif, S.; Koshy, S.T.; Darnell, M.C.; Mooney, D.J. Injectable, Tough Alginate Cryogels as Cancer Vaccines. *Adv. Healthc. Mater.* **2018**, *7*, e1701469. [CrossRef] [PubMed]

35. Koshy, S.; Zhang, D.; Grolman, J.; Stafford, A.; Mooney, D. Injectable nanocomposite cryogels for versatile protein drug delivery. *Acta Biomater.* **2017**, *65*, 36–43. [CrossRef] [PubMed]

36. Béduer, A.; Braschler, T.; Peric, O.; Fantner, G.E.; Mosser, S.; Fraering, P.C.; Benchérif, S.; Mooney, D.J.; Renaud, P. A Compressible Scaffold for Minimally Invasive Delivery of Large Intact Neuronal Networks. *Adv. Healthc. Mater.* **2015**, *4*, 301–312. [CrossRef]

37. Balkız, G.; Pingo, E.; Kahya, N.; Kaygusuz, H.; Erim, F.B. Graphene Oxide/Alginate Quasi-Cryogels for Removal of Methylene Blue. *Water Air Soil Pollut.* **2018**, *229*, 131. [CrossRef]

38. Voo, W.-P.; Lee, B.-B.; Idris, A.; Islam, A.; Tey, B.-T.; Chan, E.-S. Production of ultra-high concentration calcium alginate beads with prolonged dissolution profile. *RSC Adv.* **2015**, *5*, 36687–36695. [CrossRef]

39. Etcheverry, M.; Cappa, V.; Trelles, J.; Zanini, G. Montmorillonite-alginate beads: Natural mineral and biopolymers based sorbent of paraquat herbicides. *J. Environ. Chem. Eng.* **2017**, *5*, 5868–5875. [CrossRef]

40. Tuncaboylu, D.C.; Okay, O. Hierarchically Macroporous Cryogels of Polyisobutylene and Silica Nanoparticles. *Langmuir* **2010**, *26*, 7574–7581. [CrossRef]

41. Rodrigues, S.C.; Salgado, C.L.; Sahu, A.; Garcia, M.P.; Fernandes, M.H.; Monteiro, F.J. Preparation and characterization of collagen-nanohydroxyapatite biocomposite scaffolds by cryogelation method for bone tissue engineering applications. *J. Biomed. Mater. Res. Part A* **2013**, *101A*, 1080–1094. [CrossRef] [PubMed]

42. Önnby, L.; Svensson, C.; Mbundi, L.; Busquets, R.; Cundy, A.; Kirsebom, H. γ-Al2O3-based nanocomposite adsorbents for arsenic(V) removal: Assessing performance, toxicity and particle leakage. *Sci. Total Environ.* **2014**, *473–474*, 207–214. [CrossRef] [PubMed]

43. Zhao, X.; Guo, B.; Wu, H.; Liang, Y.; Ma, P.X. Injectable antibacterial conductive nanocomposite cryogels with rapid shape recovery for noncompressible hemorrhage and wound healing. *Nat. Commun.* **2018**, *9*, 2784. [CrossRef]

44. Shirbin, S.J.; Karimi, F.; Chan, N.J.-A.; Heath, D.E.; Qiao, G.G. Macroporous Hydrogels Composed Entirely of Synthetic Polypeptides: Biocompatible and Enzyme Biodegradable 3D Cellular Scaffolds. *Biomacromolecules* **2016**, *17*, 2981–2991. [CrossRef] [PubMed]

45. Suner, S.S.; Demirci, S.; Yetiskin, B.; Fakhrullin, R.; Naumenko, E.; Okay, O.; Ayyala, R.S.; Sahiner, N. Cryogel composites based on hyaluronic acid and halloysite nanotubes as scaffold for tissue engineering. *Int. J. Biol. Macromol.* **2019**, *130*, 627–635. [CrossRef]

46. El-Naggar, M.E.; Abdelgawad, A.M.; Tripathi, A.; Rojas, O.J. Curdlan cryogels reinforced with cellulose nanofibrils for controlled release. *J. Environ. Chem. Eng.* **2017**, *5*, 5754–5761. [CrossRef]

47. Almeida, C.; Debacher, N.; Downs, A.; Cottet, L.; Mello, C.A.D. Removal of Methylene Blue from Colored Effluents by Adsorption on Montmorillonite Clay. *J. Colloid Interface Sci.* **2009**, *332*, 46–53. [CrossRef] [PubMed]

48. Tong, D.S.; Wu, C.W.; Adebajo, M.O.; Jin, G.C.; Yu, W.H.; Ji, S.F.; Zhou, C.H. Adsorption of methylene blue from aqueous solution onto porous cellulose-derived carbon/montmorillonite nanocomposites. *Appl. Clay Sci.* **2018**, *161*, 256–264. [CrossRef]

49. Pawar, R.R.; Gupta, P.; Sawant, S.Y.; Shahmoradi, B.; Lee, S.-M. Porous synthetic hectorite clay-alginate composite beads for effective adsorption of methylene blue dye from aqueous solution. *Int. J. Biol. Macromol.* **2018**, *114*, 1315–1324. [CrossRef] [PubMed]

50. Pandey, L.M. Enhanced adsorption capacity of designed bentonite and alginate beads for the effective removal of methylene blue. *Appl. Clay Sci.* **2019**, *169*, 102–111. [CrossRef]

51. Li, Q.; Li, Y.; Ma, X.; Du, Q.; Sui, K.; Wang, D.; Wang, C.; Li, H.; Xia, Y. Filtration and adsorption properties of porous calcium alginate membrane for methylene blue removal from water. *Chem. Eng. J.* **2017**, *316*, 623–630. [CrossRef]

52. Loo, S.-L.; Lim, T.-T.; Krantz, W.B.; Fane, A.G.; Hu, X. Potential evaluation and perspectives on using sponge-like superabsorbent cryogels for onsite water treatment in emergencies. *Desalin. Water Treat.* **2015**, *53*, 1506–1515. [CrossRef]

53. Belhouchat, N.; Zaghouane-Boudiaf, H.; Viseras, C. Removal of anionic and cationic dyes from aqueous solution with activated organo-bentonite/sodium alginate encapsulated beads. *Appl. Clay Sci.* **2017**, *135*, 9–15. [CrossRef]